Mixed-valence Cu-based Heterostructure for Efficient Electrochemical Nitrate Reduction to Ammonia

Jingrui Ye, Yilin Yang, Mengjuan Teng, An Wang, Jiawei Xia, Guangyu He*and Haiqun Chen*

Determination of ion concentrations

The ultraviolet-visible (UV-Vis) spectrophotometer was employed to analyze the concentrations of NO_3^--N, NO_2^--N, and NH_4^+-N, the corresponding concentration-absorbance curves were shown in Figure S1, S2 and S3.

Determination of NO_3^--N

The concentration of NO_3^--N in electrolyte was determined before and after chronoamperometry tests. Specifically, 1 M HCl (0.1 mL) and 0.8 wt.% sulfamic acid solution (0.01 mL) were added to the diluted electrolyte. UV-Vis spectrophotometer was employed to record absorption spectrum and the absorbance intensities at wavelength of 220 and 275 nm were used to determine the concentration of NO_3^-N ($A = A_{220nm} - 2A_{275nm}$). The concentration-absorbance standard curve was calibrated by using various KNO_3 aqueous solutions as the standard samples in the same operation.

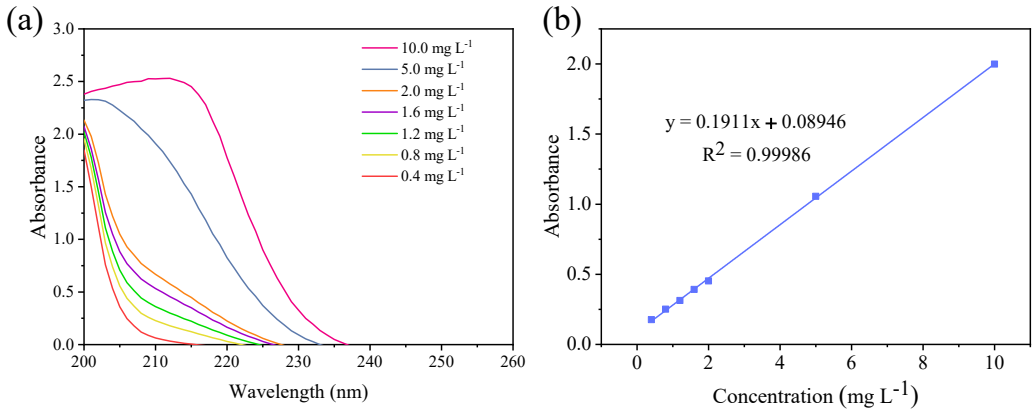

Fig. S1 UV-Vis curves and concentration-absorbance calibration curves of NO_3^--N

Determination of NO_2^--N

The concentration of NO_2^--N in electrolyte was determined by Griess test according to the literature. The absorbance intensity at a wavelength of 540 nm in UV-Vis spectrum was recorded to determine the concentration of NO_2^--N. The concentration-absorbance standard curve was calibrated by using various $NaNO_2$ aqueous solutions as the standard samples in the same operation.

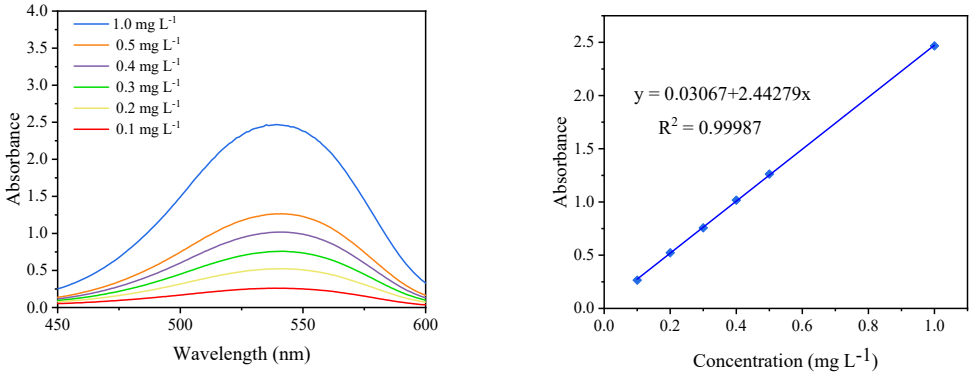

Fig. S2 UV-Vis curves and concentration-absorbance calibration curves of NO_2^--N

Determination of NH_4^+

The concentration of generated NH_3 was determined by quantitative detection of NH_4^+ in electrolyte using the indophenol blue (IB) method. In this method, NH_4^+ reacts with phenols and hypochlorite (ClO^-) in a strongly alkaline medium to form IB, with nitroprusside acting as a catalyst. Specifically, 14.1 g of phenol and 163 mg of sodium nitroprusside ($Na[Fe(NO)(CN)_5]$) were mixed and diluted to 1L with water, which was marked as solution A. 5.2 g of NaOH and 3.07 mL of NaClO were mixed and diluted to 1L with water, which was marked as solution B. To determine the concentration of NH_4^+, 2.5 mL of solution A and 2.5 mL of solution B were added to 1.0 mL of diluted electrolyte. The absorbance intensity at a wavelength of 623 nm in UV-Vis spectrum was recorded. The concentration-absorbance standard curve was calibrated by using various ammonium chloride solutions as the standard samples in the same operation.

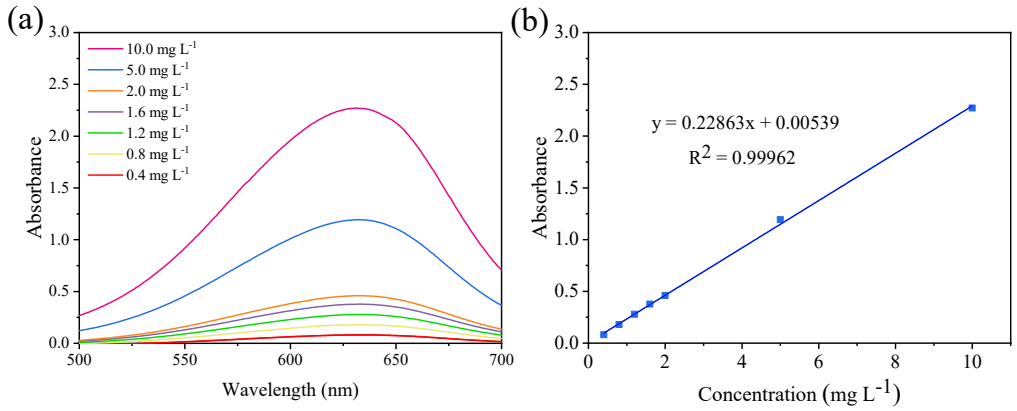

Fig. S3 UV-Vis curves and concentration-absorbance calibration curves of NH_4^+-N

Calculations

The NO_3^- removal efficiency *($R(NO_3^-\text{-}N)$)*, NO_2^--N selectivity *($S(NO_2^-\text{-}N)$)*, NH_4^+-N selectivity *($S(NH_4^+\text{-}N)$)*, selectivity of other product *($S(others)$)*, yield rate and Faraday efficiency of ammonia (*FE*) were calculated by following equations:

$$R(NO_3^-) = \frac{C_0\,(NO_3^-\text{-}N) - C_t\,(NO_3^-\text{-}N)}{C_0\,(NO_3^-\text{-}N)} \times 100\%$$

$$S(NO_2^-) = \frac{C_t\,(NO_2^-\text{-}N)}{C_0\,(NO_3^-\text{-}N) - C_t\,(NO_3^-\text{-}N)} \times 100\%$$

$$S(NH_4^+) = \frac{C_t(NH_4^+\text{-}N)}{C_0\,(NO_3^-\text{-}N) - C_t\,(NO_3^-\text{-}N)} \times 100\%$$

$$S(others) = \frac{C_0\,(NO_3^-\text{-}N) - C_t\,(NO_3^-\text{-}N) - C_t\,(NO_2^-\text{-}N) - C_t(NH_4^+\text{-}N)}{C_0\,(NO_3^-\text{-}N) - C_t\,(NO_3^-\text{-}N)} \times 100\%$$

$$Yield = \frac{C_t(NH_4^+\text{-}N) \times V}{t \times A \times M_N} \times 10^{-3}$$

$$FE = \frac{8 \times F \times C_t(NH_4^+\text{-}N) \times V \times 10^{-6}}{M_N \times Q} \times 100\%$$

Where $C_0\ (NO_3^-\text{-}N)$ represents the initial concentration of NO_3^- - N. $C_t\ (NO_3^-\text{-}N)$, $C_t\ (NO_2^-\text{-}N)$, and $C_t(NH_4^+\text{-}N)$ represent the measured concentration of NO_3^- - N, NO_2^- - N, and NH_4^+ - N at reaction time t (h), respectively, V is the electrolyte volume in the cathode chamber (35 mL), A is the geometric area of the electrode (1.0 cm^2), M_N is the molar mass of N, F is the Faraday constant (96 485 C mol^{-1}), and Q is the total charge during electrolysis.

The electrochemical surface area (ECSA) was calculated by followed equation:

$$C_{dl} = \frac{I_c}{v}$$

$$ECSA = \frac{C_{dl}}{C_s}$$

where C_{dl} is capacitance of double layer of electrode determined by CVs at different scan rates, I_c is current in CV, v is scan rate. Specifically, C_{dl} was estimated by plotting the difference of cathode and anode current density to scanning rate, where the slope is twice that of C_{dl}. C_s is the ideal specific capacitance and use general value in alkaline solutions (40 μF cm^{-2} per cm_{ECSA}).

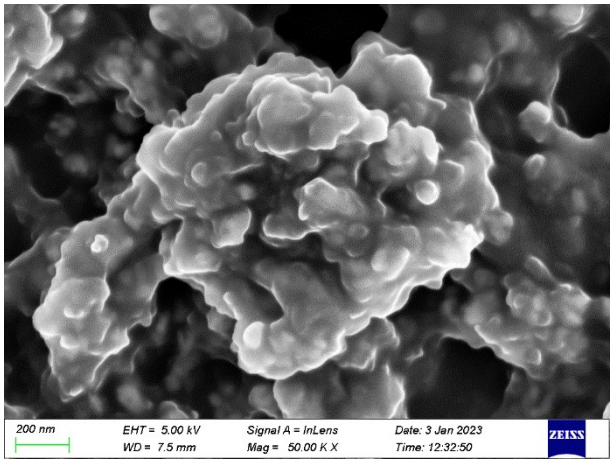

Fig. S4 SEM image of Cu-Cu_xO/C

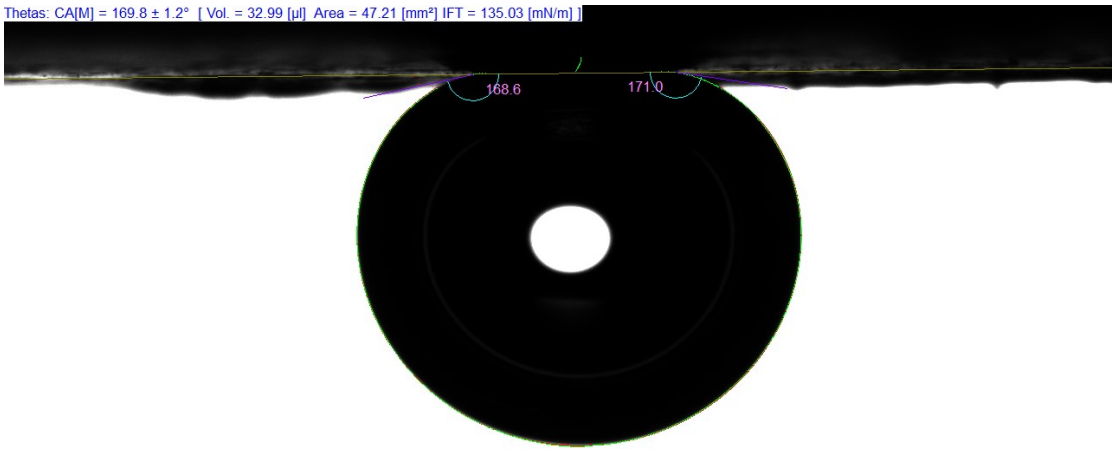

Fig. S5 The contact angle of Cu-Cu_xO/C-0.3

Table S1 The atomic ratios of [(Cu^0+Cu^+)/Cu^{2+}] of Cu-Cu_xO/C, Cu-Cu_xO/C-0.1, Cu-Cu_xO/C-0.3 and Cu-Cu_xO/-0.5 catalysts

Catalyst	(Cu^0+Cu^+)/Cu^{2+}
Cu-CuxO/C	0.14
Cu-CuxO/C-0.1	0.36
Cu-CuxO/C-0.3	2.60
Cu-CuxO/C-0.5	0.33

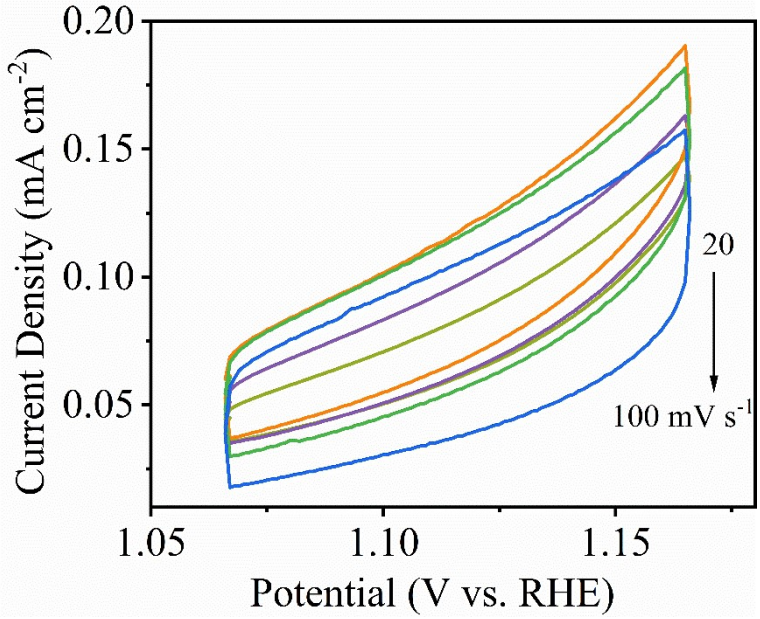

Fig. S6 CV curves of Cu-Cu_xO/C under the scan rates of 20~100 mV s^{-1} at 1 M KOH with 0.1 M NO_3^-

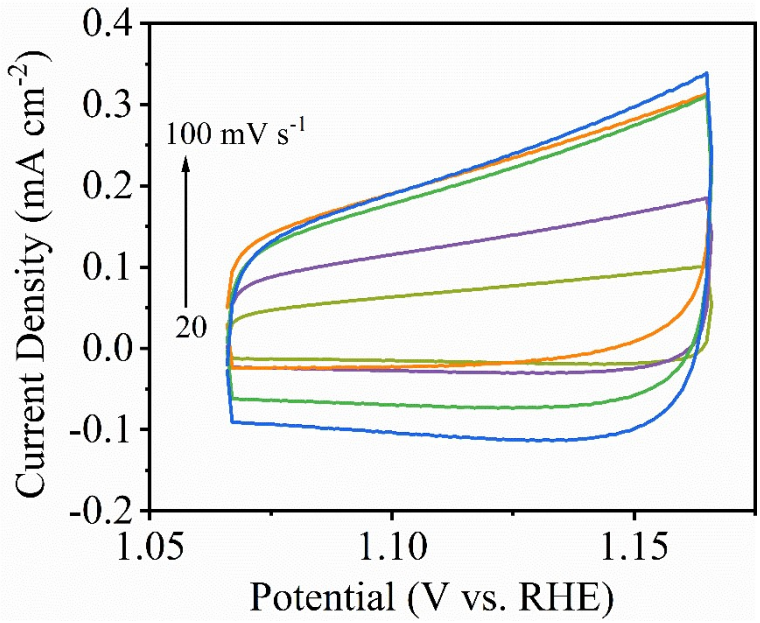

Fig. S7 CV curves of Cu-Cu_xO/C-0.1 under the scan rates of 20~100 mV s^{-1} at 1 M KOH with 0.1 M NO_3^-

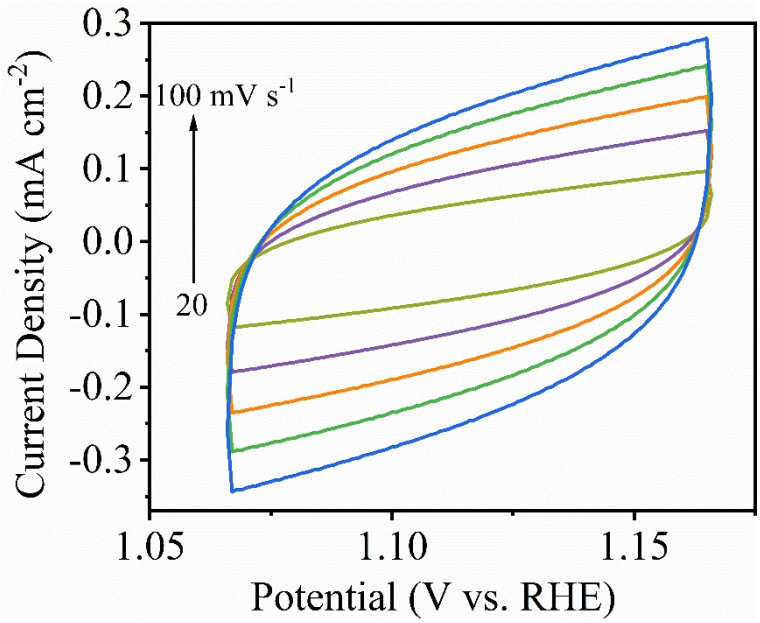

Fig. S8 CV curves of Cu-Cu_xO/C-0.3 under the scan rates of 20~100 mV s^{-1} at 1 M KOH with 0.1 M NO_3^-

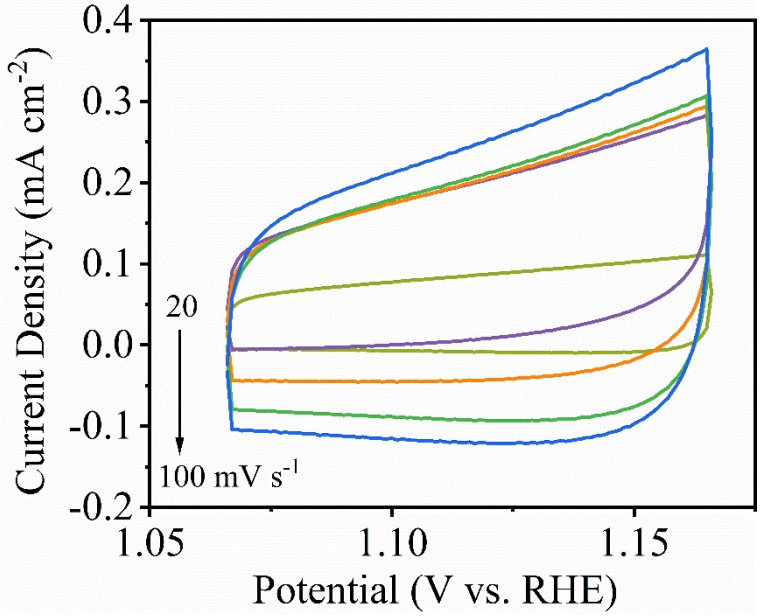

Fig. S9 CV curves of Cu-Cu_xO/C-0.5 under the scan rates of 20~100 mV s^{-1} at 1 M KOH with 0.1 M NO_3^-

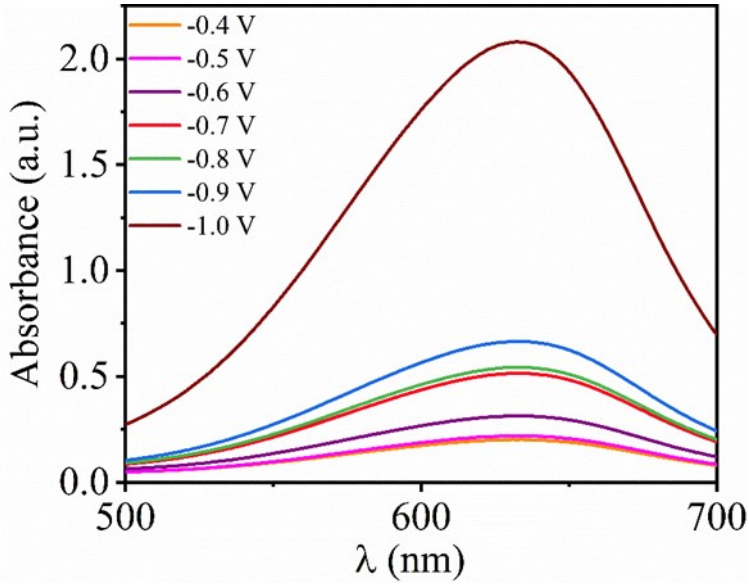

Fig. S10 UV spectra of Cu-Cu_xO/C-0.3

Table S2 The detailed comparison of NO_3RR performance of recently reported Cu-based catalysts and Cu_2S-CuO/NC

Catalysts	Yield rate	FE	Electrolyte	Potential	Ref.
Co_3O_4/Cu	684 μg $mg_{cat.}^{-1}$ h^{-1}	94.60%	0.4 M Na_2SO_4 with 50 mg L^{-1} NO^{3-}-N	−0.4 V vs. RHE	[1]
CuO@PANI/CF	0.213 mmol h^{-1}	93.88%	0.5 M K_2SO_4 with 200 ppm NO^{3-}-N	−0.95 V vs. SCE	[2]
$CuCo_2O4$/CFs	394.5 mmol h^{-1} g^{-1}	81.90%	1 M KOH with 0.1 M NO^{3-}	−0.3 V vs. RHE	[3]
Cu@$Cu_{2+1}O$ NWs	576.53 μg h^{-1} $mg_{cat.}^{-1}$	87.07%	0.5 M K_2SO_4 with 50 mg L^{-1} KNO_3	−1.2 V vs. SCE	[4]
TiO_2 NTs/CuO	1241.81 μg h^{-1} cm^{-2}	92.23%	0.5 M Na_2SO_4 with 100 ppm KNO_3-N	−0.75 V vs. RHE	[5]
Cu nanosheets	1.41 mmol h^{-1} cm^{-2}	>80 %	1 M KOH with 0.2 M KNO_3 solution	−0.59 V vs. RHE	[6]
Cu/Pd/CuO_x heterostructures	1510.3 μg h^{-1} $mg_{cat.}^{-1}$	84.04%	0.5 M K_2SO_4 with 50 mg L^{-1} KNO_3-N	−1.3 V vs. SCE	[7]
Cu/MnO_x Hybrids	29.3 mg h^{-1} $mgcat.^{-1}$	86.20%	0.1 M Na_2SO_4 with 100 mM KNO_3	−0.6 V vs. RHE	[8]
Cu/MnO_x Hybrids	5.53 mg h^{-1} $mg_{cat.}^{-1}$	98.20%	0.1 M Na_2SO_4 with 10 mM KNO_3	−0.7 V vs. RHE	[9]
Cu-N-C SAC	4.5 mg cm^{-2} h^{-1} (12.5 mol_{NH3} g_{Cu}^{-1} h^{-1})	84.70%	0.1 M KOH with 0.1 M KNO_3	−1.00 V vs. RHE	[10]
Cu_2O	0.0699 mmol h^{-1} mg^{-1}	85.26%	0.5 M sodium sulfate with 200 ppm nitrate	−1.2 V vs. RHE	[11]
oxide-derived Cu	1.1 mmol h^{-1} cm^{-2}	92%	1 M KOH with 100 mM NO^{3-}	−0.15 V vs. RHE	[12]
$Cu_{50}Ni_{50}$	583.6 ± 2.4 μmol cm^{-2} h^{-1}	88.0 ± 1.6%	1 M KOH with 100 mM KNO_3	−1.2 V vs. RHE	[13]
Ru@C_3N_4/Cu	0.249 mmol h^{-1} cm^{-2}	-	0.5 M Na_2SO_4 with NO^{3-}	−0.9 V vs. RHE	[14]
Cu-Cu_xO/C-0.3	13.38 mg_{NH3-N} cm^{-2} h^{-1} (ca. 2.39 mol $g_{cat.}^{-1}$ h^{-1})	81.4%	1 M KOH with 100 mM KNO_3	−0.8 V vs. RHE	This work
Cu-Cu_xO/C-0.3	17.64 mg_{NH3-N} cm^{-2} h^{-1} (ca. 3.15 mol $g_{cat.}^{-1}$ h^{-1})	79.9%	1 M KOH with 100 mM KNO_3	−1.0 V vs. RHE	This work

References

[1] W. Fu, Z. Hu, Y. Du, P. Su, Y. Su, Q. Zhang, M. Zhou, Building dual active sites Co_3O_4/Cu electrode

to break scaling relations for enhancement of electrochemical reduction of nitrate to high-value ammonia, J. Hazard. Mater. 434 (2022) 128887, https://doi.org/10.1016/j.jhazmat.2022.128887.

[2] Y. Xu, Y. Wen, T. Ren, H. Yu, K. Deng, Z. Wang, X. Li, L. Wang, H. Wang, Engineering the surface chemical microenvironment over CuO nanowire arrays by polyaniline modification for efficient ammonia electrosynthesis from nitrate,Appl. Catal. B: Environ. 320 (2023) 121981, https://doi.org/10.1016/j.apcatb.2022.121981.

[3] Z. Niu, S. Fan, X. Li, P. Wang, Z. Liu, J. Wang, C. Bai, D. Zhang, Bifunctional copper-cobalt spinel electrocatalysts for efficient tandem-like nitrate reduction to ammonia, Chem. Eng. J. 450 (2022) 138343, https://doi.org/10.1016/j.cej.2022.138343.

[4] T. Ren, K. Ren, M. Wang, M. Liu, Z. Wang, H. Wang, X. Li, L. Wang, Y. Xu, Concave-convex surface oxide layers over copper nanowires boost electrochemical nitrate-to-ammonia conversion, Chem. Eng. J. 426 (2021) 130759, https://doi.org/10.1016/j.cej.2021.130759.

[5] W. Qiu, X. Chen, Y. Liu, D. Xiao, P. Wang, R. Li, K. Liu, Z. Jin, P. Li, Confining intermediates within a catalytic nanoreactor facilitates nitrate-to-ammonia electrosynthesis, Appl. Catal. B: Environ. 315 (2022) 121548, https://doi.org/10.1016/j.apcatb.2022.121548.

[6] Y. Fu, S. Wang, Y. Wang, P. Wei, J. Shao, T. Liu, G. Wang, X. Bao, Enhancing Electrochemical Nitrate Reduction to Ammonia over Cu Nanosheets via Facet Tandem Catalysis, Angew. Chem. Int. Ed. 62 (26) (2023) e202303327, https://doi.org/10.1002/anie.202303327.

[7] T. Ren, Z. Yu, H. Yu, K. Deng, Z. Wang, X. Li, H. Wang, L. Wang, Y. Xu, Interfacial polarization in metal-organic framework reconstructed Cu/Pd/CuO_x multi-phase heterostructures for electrocatalytic nitrate reduction to ammonia, Appl. Catal. B: Environ. 318 (2022) 121805, https://doi.org/10.1016/j.apcatb.2022.121805.

[8] Y. Cui, A. Dong, Y. Zhou, Y. Qu, M. Zhao, Z. Wang, Q. Jiang, Interfacially engineered nanoporous Cu/MnO_x hybrids for highly efficient electrochemical ammonia synthesis via nitrate reduction, Small 19 (17) (2023) 2207661, https://doi.org/10.1002/smll.202207661.

[9] J. Yang, H. Qi, A. Li, X. Liu, X. Yang, S. Zhang, Q. Zhao, Q. Jiang, Y. Su, L. Zhang, J. Li, Z. Tian, W. Liu, A. Wang, T. Zhang, Potential-Driven restructuring of cu single atoms to nanoparticles for boosting the electrochemical reduction of nitrate to ammonia, J. Am. Chem. Soc. 144 (27) (2022) 12062-12071, https://doi.org/10.1021/jacs.2c02262.

[10] Z. Gong, W. Zhong, Z. He, Q. Liu, H. Chen, D. Zhou, N. Zhang, X. Kang, Y. Chen, Regulating

surface oxygen species on copper (I) oxides via plasma treatment for effective reduction of nitrate to ammonia, Appl. Catal. B: Environ. 305 (2022) 121021, https://doi.org/10.1016/j.apcatb.2021.121021.

[11] J. Yuan, Z. Xing, Y. Tang, C. Liu, Tuning the oxidation state of cu electrodes for selective electrosynthesis of ammonia from nitrate, ACS Appl. Mater. Inter. 13 (44) (2021) 52469-52478, https://doi.org/10.1021/acsami.1c10946.

[12] Y. Bu, C. Wang, W. Zhang, X. Yang, J. Ding, G. Gao, Electrical Pulse-Driven periodic Self-Repair of Cu-Ni tandem catalyst for efficient ammonia synthesis from nitrate, Angew. Chem. Int. Ed. 62 (24) (2023) e202217337, https://doi.org/10.1002/anie.202217337.

[13] Y. Zheng, M. Qin, X. Yu, H. Yao, W. Zhang, G. Xie, X. Guo, Constructing ru@C_3N_4/Cu tandem electrocatalyst with Dual-Active sites for enhanced nitrate electroreduction to ammonia, Small 19 (30) (2023) 2302266, https://doi.org/10.1002/smll.202302266.